Generating and Comparing Dark Matter Distributions in the Merging and Non-Merging Galaxy Clusters Abell 1651 and Abell 1650

by

Quentin Edens

Bachelors of Science in Physics

Brown University

2021

TABLE OF CONTENTS(?)

LIST OF FIGURES

ACKNOWLEDGEMENTS

I would like to express my gratitude and deepest appreciation to my thesis supervisor, Professor Ian Dell'antonio, for his patience, guidance, and encouragement in facilitating all of the learning and image processing necessary in completing this thesis. Without his assistance in enabling my learning and providing advice in my writing, I surely would not have been able to achieve this feat.

Furthermore, I would like to extend my sincerest thanks to Research and Teaching Assistant Shenming Fu for writing all of the code necessary in providing a framework for my research. Similarly, without his continuous support in bug-fixing and optimizing the processing, I certainly would not have been able to complete this analysis.

Chapter 1. Introduction:

Despite constituting approximately a quarter of the composition of our universe, dark matter remains as one of the most elusive structures known to us. This fact maintains true for good reason; dark matter acts neither like traditional baryonic matter, nor does it have the telltale high-energy properties of antimatter. Although we cannot directly view it, as it does not interact with light in the traditional form of absorption and emission, we can begin to parameterize both its structure and how it interacts with baryonic matter through gravitational lensing. In particular, we look at the gravitational lensing of galaxy clusters in order to discern the structure and behavior of dark matter; this choice is made for several reasons: Firstly, galaxy clusters contain a lot of dark matter, thus making it relatively easier to measure than other objects due to the correspondingly stronger lensing signals. Secondly, in trying to glean insight into how dark matter acts during merging events, galaxy clusters are used because they are the most frequent mergers available to us. In considering mergers between galaxies instead, they simply aren't frequent enough in our current epoch to provide large enough sample sizes, and therefore allow us to draw any substantial conclusions. Finally, galaxy clusters form late in the universe, yet are large enough such that they may still preserve the history of their formation within its structure. Therefore, in studying the properties and distributions of dark matter within clusters, we may also be able to learn about how the sub-structure of dark matter originates and changes throughout the evolution of galaxy clusters.

The clusters chosen in this study were taken from Abell's catalogue of galaxy clusters, which consists of just over 4,000 low-redshift ($z \leq 0.2$) clusters. Among this catalogue, Abell 1651(A1651) and Abell 1650(A1650) were chosen to compare in this paper. While the characterization of galaxy clusters does not yet have a robust classification system, the two clusters were chosen to compare because A1651 is in the process of merging with another cluster, while A1650 is not. Therefore, the analysis of this paper largely consists of comparing how dark matter distributions change in the context of merging clusters.

In terms of what is actually done in analyzing the clusters, I used Brown's supercomputer Oscar in tandem with Professor Dell'antonio's research with the Dark Energy Telescope in Chile to analyze CCD imagery of galaxy clusters in order to produce dark matter distributions. In particular, we looked at the degree of co-location between the distributions of luminous matter

and dark matter, as well as any larger sub-structure the dark matter may take within the cluster. Preliminarily, our expectation is that the merging cluster, A1651, will have a lower degree of co-location between luminous and dark matter, and furthermore that merging clusters will have more local sub-maxima lensing signals, corresponding to a 'lumpier' dark matter distribution, due to the timescale at which cluster mergers occur. In particular, since the time it takes for a merging event to conclude is on the scale of billions of years, we expect that the merging cluster will have a lumpier dark matter distribution because it has not had enough time to reassemble into a smooth distribution.

Chapter 2. Background:

The only theoretical background necessary in this paper follows (Wittman, 2002), which concerns using the measured shapes of galaxies to insinuate the degree of gravitational lensing occurring. Traditionally, in considering the gravitational lensing of an object, we can begin with the inverse magnification matrix:

$$M^{-1} = (1-\kappa)\begin{pmatrix}1 & 0\\ 0 & 1\end{pmatrix} + \gamma\begin{pmatrix}\cos(2\phi) & \sin(2\phi)\\ \sin(2\phi) & -\cos(2\phi)\end{pmatrix}$$

Which describes the change in source coordinates for an infinitesimal change in image coordinates. Here, κ is the convergence, which represents an isotropic magnification of the object, and γ is the shear, which corresponds to stretching in the ϕ direction. While κ can be interpreted simply as the projected mass density divided by a critical density, γ is non-local, and thus its value at a given position on the sky depends on the mass distribution everywhere. Therefore, in order to determine the degree of gravitational lensing, we must either analyze a source distribution, or measure galaxy shape distributions. Between the two, measuring galaxy shape distribution is generally preferred due to its ability to measure departures from zero, rather than measuring small changes in big numbers, as is the case with looking at source distributions. In looking at galaxy shape distributions, we begin by approximating each galaxy as an ellipse with position angle ϕ and ellipticity:

$$\epsilon = \frac{b^2 - a^2}{(a^2 + b^2)}$$

Where a and b are the semimajor and semiminor axes respectively. From this, we can define a vector ellipticity:

$$e_i = (\epsilon \cos(2\phi), \epsilon \sin(2\phi))$$

Which encodes the position angle and scalar ellipticity into two comparable quantities. Furthermore, the dependence on 2ϕ means that the quantity is invariant under 180-degree rotations. By observing the distribution of e_i in locations far from any known lens, we have found that the distribution is roughly Gaussian with zero mean. Therefore, any departure of e_i from zero is assumed to be due to lensing. It should be noted, however, that the previous statement is founded on the assumption that galaxy orientation is random in the absence of lensing, although this is believed to be a solid assumption.

Chapter 3. Methods:

The process of observing and measuring dark matter begins with taking many images of a given galaxy cluster using the Dark Energy Survey's telescope. The telescope, which consists of 62 CCDs, varies both with respect to the filter chosen as well as the orientation of the telescope. Several images are taken in each filter, slightly shifted by position, to account for spaces in between each CCD; this later allows us to create a composite image without any discontinuities. As seen in Figure 1, the five primary filters used are u, g, r, i, and z. While the majority of the analysis in this paper involves the r-band, the other bands are necessary in order to fill out the rest of the visible spectrum.

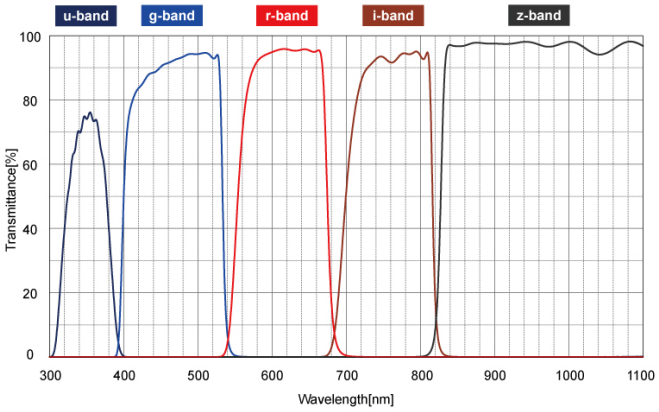

Figure 1: The filters used in imaging the galaxy clusters. In addition to the five shown, there is also Y and VR, which occupy slightly different regions of this same spectrum

With an inventory of many pictures differing in position and filter, we begin a stage of processing in order to correct any noise seen within the pictures. Typical correction at this stage involves accounting for pixel-to-pixel variance in efficiency and removing the contribution of the night sky. In doing so, images of the sky divided up into 62 cells are created, corresponding to each CCD, as seen in Figure 2. With these images, a further stage of correction is undergone in which a quality check is done by hand to further weed out other aspects which may contribute to poor picture quality. Typical sources of noise which we searched for during this stage are weather, detector failures, satellite trails, and failures of the previous processing step in either removing the night sky or accounting for variance in pixel efficiencies. With respect to this, Figure 2 provides a good example of many of the types of errors which are checked for. There are other images, such as the one in Figure 3, which have too many detector failures to be salvagable and thus must be deleted all together.

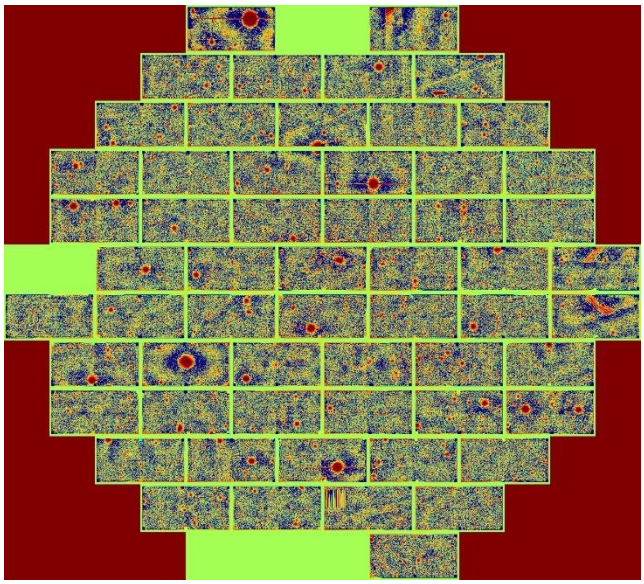

Figure 2: Images after processing. The top-middle and bottom-middle cells are always left empty, thus the cells missing on the left and bottom left are the only two which failed. Satellite trails can be seen as straight lines toward the top-right of the image.

Before continuing with further processing of the images, we perform another stage of quality control in which the eccentricity and size of nearby stars are evaluated within each cell. To begin with the prior, the eccentricity of nearby stars is measured to account for any intrinsic eccentricity produced by the telescope as a result of incorrect focus. Stars are used as a reference in this step because they are easily distinguishable, and should be spherical. This is then graphed, as seen in Figure 4, spatially onto each part of every image in order to observe which parts of each image are in poor focus.

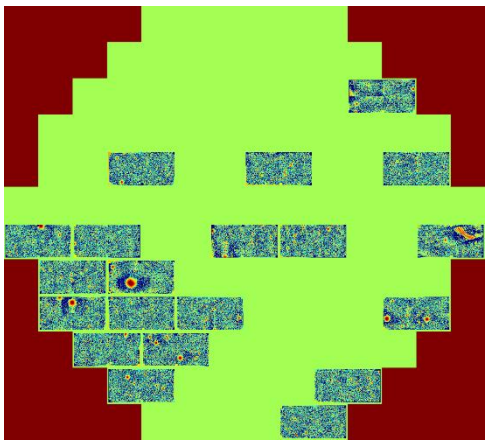

Figure 3: Example in which over half of the total cells failed, resulting in exclusion of the entire image in further processing

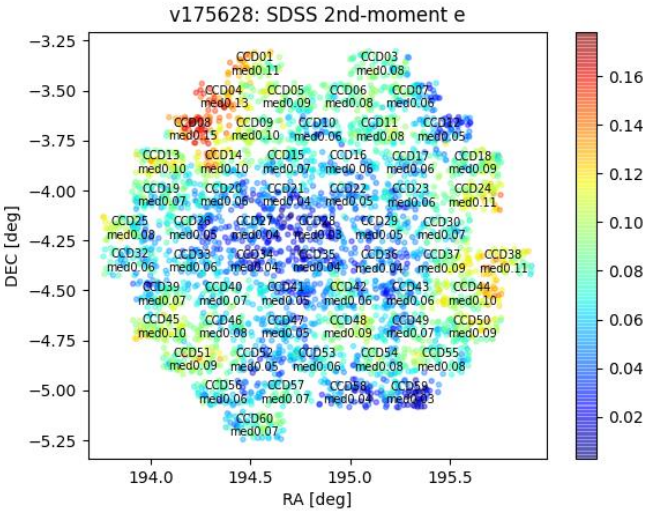

Figure 4: Eccentricity of stars identified within each cell. Blue corresponds to low eccentricity, which is desired. Red corresponds to high eccentricity, which must be excluded from further processing if it is too pervasive throughout the image

The value in checking for such errors comes into play later on in analyzing the results, as the ellipticity of galaxies is one of the key measurements needed for our analysis. A similar graph is produced for star size with respect to each cell, in which cells with stars that are too big are excluded from further processing. This is done in order to minimize distortion in the shapes of objects within the image, as atmospheric turbulence of larger stars can begin to have a significant effect on measurements. Similar to the previous reasoning, atmospheric turbulence must be mitigated because galaxy shape plays a critical role in our analysis, and thus must be accurate in order to draw reasonable conclusions.

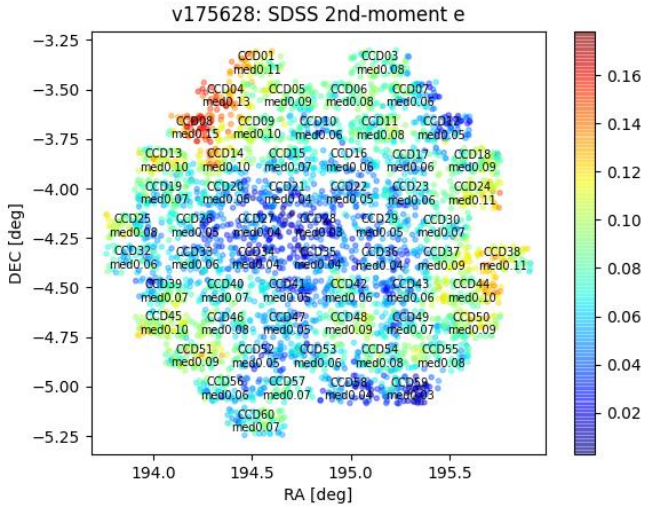

Figure 5: Size of stars within each cell. Similar to Fig. 4, blue corresponds to low sizes, which is desirable. Red corresponds to large star sizes, which must be excluded if it is significant enough to harm analysis.

After mitigating errors intrinsic to our measurements, we begin to compile a single smooth image of the sky in order to start establishing a galaxy catalogue. The process of compilation involves using the GAIA satellite reference catalogue to first establish a common agreement of star locations among each image. Afterwards, a second catalogue from the Pan-STARRS survey is used to calibrate image brightness as a function of position, and accordingly scale the intensity of each image. From the reference points established by the GAIA catalogue, a transformation function is calculated for each image, which maps the position of each region of the original images to a new point on the compiled image. This process is repeated in order to align each image, thereby creating a single smooth composite image, as seen in Figure 6.

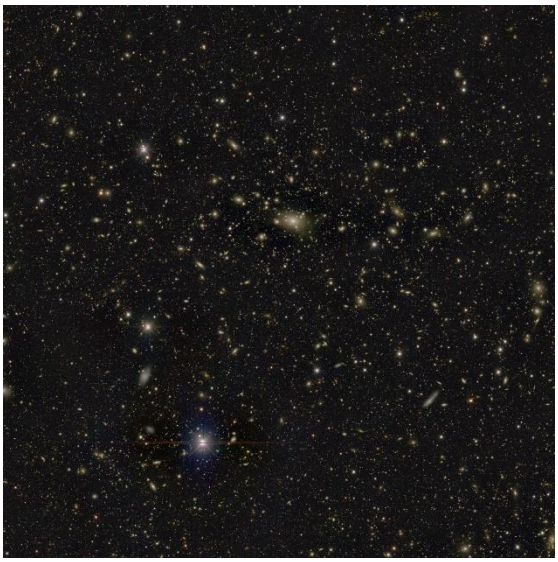

Figure 6: Composite image of the cluster in visible light.

With a composite image, we begin to create a catalogue of galaxies within the cluster in order to start taking measurements. The first step taken in creating a catalogue involves identifying areas within the image above a certain light threshold; this acts to create a preliminary list of suspect objects to be further characterized. Using the aforementioned suspect list, the next step of processing consists of deblending objects which may occupy the same region, and therefore contribute to the same catalogued light threshold. Figure 7 shows a zoomed-in view of the compiled image, in which examples where deblending is necessary can be seen.

With the deblended catalogue, we begin to take measurements of our galaxies. In particular, the two measurements calculated and used are the ellipticity and brightness of each galaxy. Furthermore, in measuring the shapes and luminosities of galaxies, stars are distinguished within the catalogue and excluded from further analysis – thus finalizing our list of relevant galaxies.

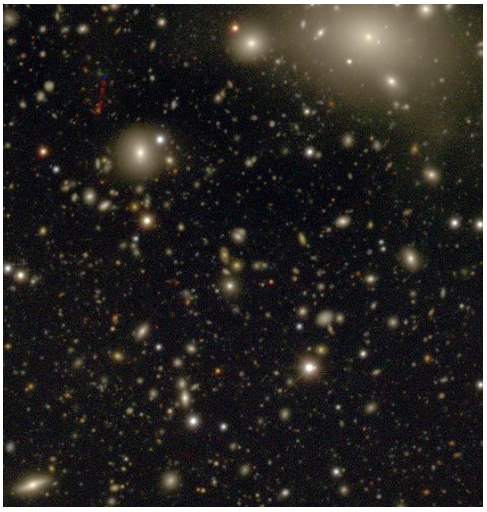

Figure 7: Zoomed-in view of the composite image previously shown. The top right of the image shows several galaxies which contribute to the same light threshold, and thus must be deblended before further analysis.

Chapter 4. Results:

X-ray/Gravitational Lensing Topology:

With a finished galaxy catalogue, we can now begin to analyze trends in properties seen throughout the cluster in order to insinuate dark matter distribution. In particular, the distribution of dark matter is generated by comparing the distribution of light, as seen in X-ray, with the strength of the gravitational lensing signal throughout the cluster. The method of generating the gravitational lensing signal consists of averaging the tangential ellipticities of each galaxy with respect to every point on the map, and repeating that process for every galaxy on the map. Assuming galaxies have random orientation, this yields information on the degree of gravitational lensing at each point on the map. By creating a topology of both the gravitational lensing signal and the X-ray emission and overlaying them onto the compiled image created earlier, we can observe the degree of co-location between the X-ray center and gravitational lensing center, as well as any larger sub-structure the dark matter may take. The result of doing so can be seen in Figure 8. It is worth noting that there are other forms of X-ray emission which may not contribute to a mass distribution estimate, such as emission from shock heating. Due to the uniformity of the X-ray topology, however, we believe that this doesn't play a significant role with respect to our measurements, as the shock emission would need to have a similarly uniform distribution to go unnoticed.

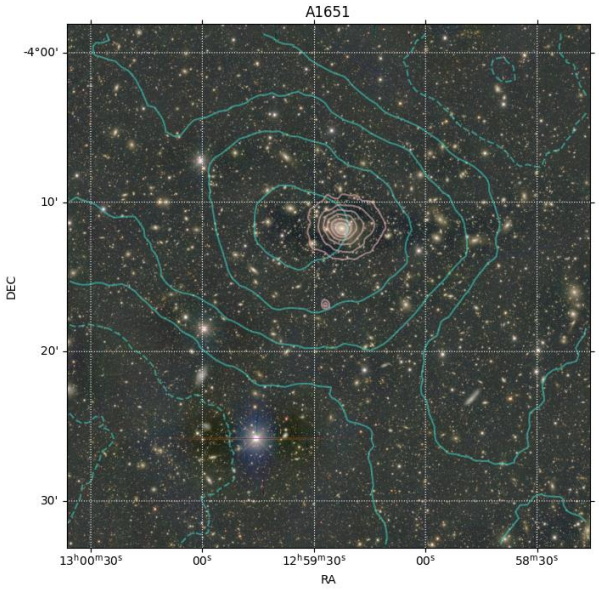

Figure 8: X-ray topology(pink) overlapped with gravitational lensing signal(blue). The dotted-blue lines represent under-dense regions of lensing signaling. The two signals are not completely co-located, suggesting the dark and luminous matter are not aligned.

Shear Profile:

An additional result which will be relevant in comparing between clusters comes from constructing a shear profile of the cluster. The profile is created by first taking the center of the galaxy cluster as seen in X-ray, and constructing concentric rings around it. Each ring, the tangential ellipticity and cross component of each galaxy within the ring is averaged. Through averaging across each ring and plotting it as a function of radius, we produce a radial shear profile, as seen in Figure 9.

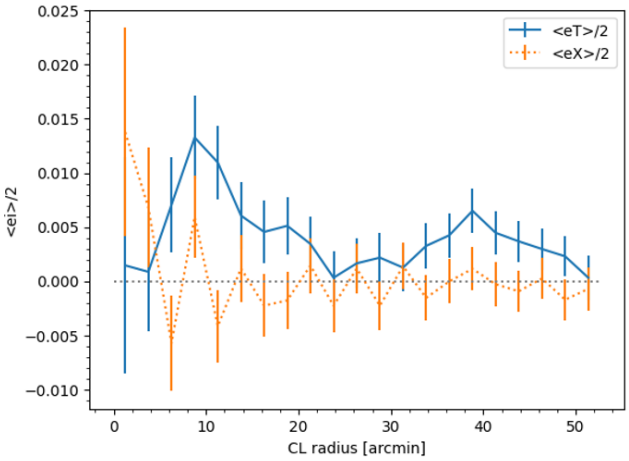

Figure 9: Radial shear profile of the galaxy cluster. The tangential ellipticity(eT) should taper toward 0 as r trends outwards, and the cross component(eX) should always remain around 0

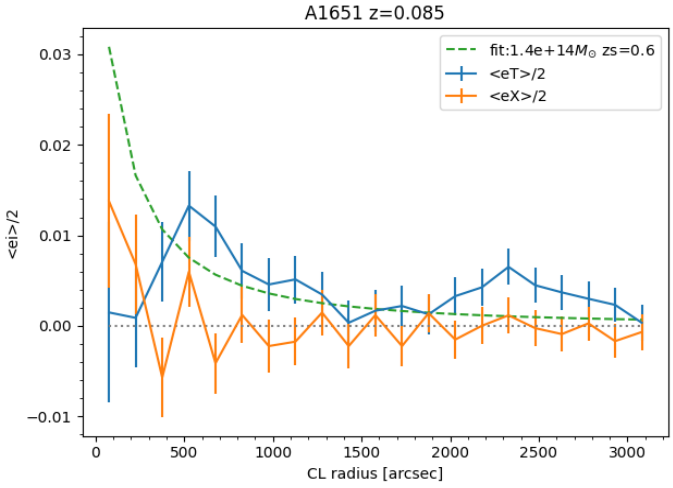

Figure 10: Mass distribution extrapolated from comparing radial shear profile with a Navarro-Frenk-White characteristic density profile

By comparing the constructed shear profile with a characteristic density profile, we can also estimate a mass distribution for the cluster, which is shown in Figure 10. The characteristic density profile used is the Navarro-Frenk-White (NFW) profile, which relates the radius of a cluster to its average density using numerical simulation. With information on the shear profile of the galaxy cluster, we can also estimate the total mass of the cluster.

Mass Histogram:

Total cluster mass is a result which, while not particularly insightful on its own, will be useful in comparing between different galaxy clusters. The cluster mass is estimated by generating a mass histogram, in which the frequency of a given mass estimate is represented over a total sample size of 1,000 estimates, as seen in Figure 11. The sample size is created by taking a random two-thirds of the galaxy catalogue, and generating a shear profile for that sub-group of galaxies. A mass estimate for the sub-group is then given by comparing the shear profile to the same NFW characteristic density profile as before. This two-thirds sampling process is then repeated 1,000 times, in order to generate 1,000 different mass estimates, which is then plotted as a function of frequency to produce the histogram.

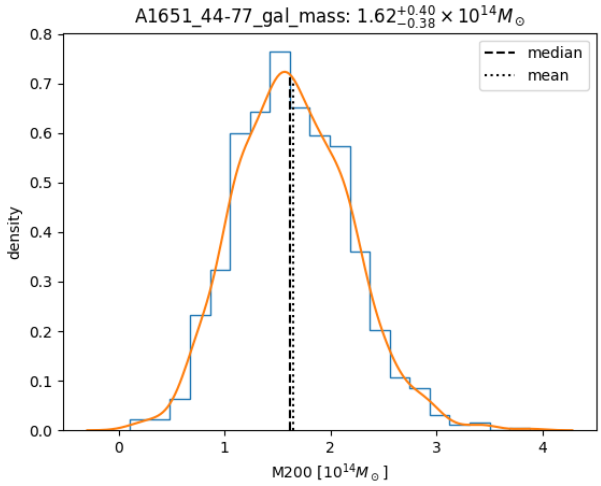

Figure 11: Histogram of frequency of mass estimates. X-axis represents mass, and y-axis shows how many times a given mass was estimated. The blue line is the actual data, and the orange line is a smoothened fit for the data.

Chapter 5. Comparing:

With these results, we can now begin to compare dark matter distributions between merging and non-merging galaxy clusters. While the only figures we necessarily care to compare are the topology maps, which allows us to observe dark matter distribution and degree of co-location, both the mass histogram and mass distribution graphs are also necessary to compare in order to limit the number of variables, and therefore begin to draw reasonable conclusions. All of the processing and output data shown thus far have been of A1651, a merging galaxy cluster. Here, we will begin to compare A1651 with A1650, which is a non-merging cluster.

In looking at how the mass histograms compare with each other, as seen in Figure 12, we can see that the two clusters are not identical in mass, but within a margin of error of each other. Comparing the mass histograms in this sense is more of a quality check than anything to glean information from, as the two clusters were initially chosen to compare because they were expected to be similar in terms of their mass.

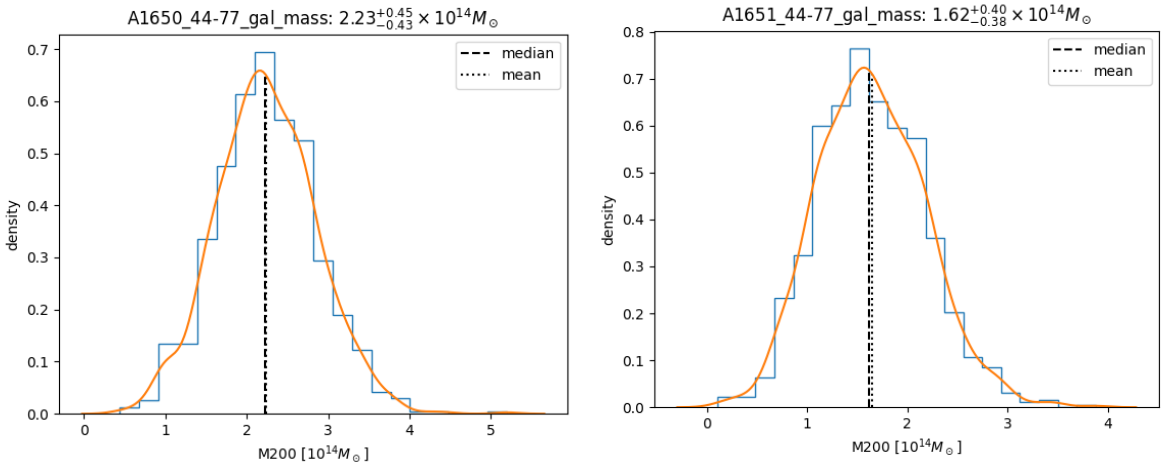

Figure 12: (Left) mass histogram of A1650. (Right) mass histogram of A1651. Both clusters share similar mass estimates, approximately within a margin of error of each other.

Comparing the two clusters' shear profiles, however, can yield new information. As seen in Figure 13, both clusters share similar mass distributions and follow the same trends we expect. Namely, both clusters have tangential ellipticities which trend toward 0 as r increases, and cross components which stay near zero. The two profiles differ, however, in how they act as we approach r = 0.

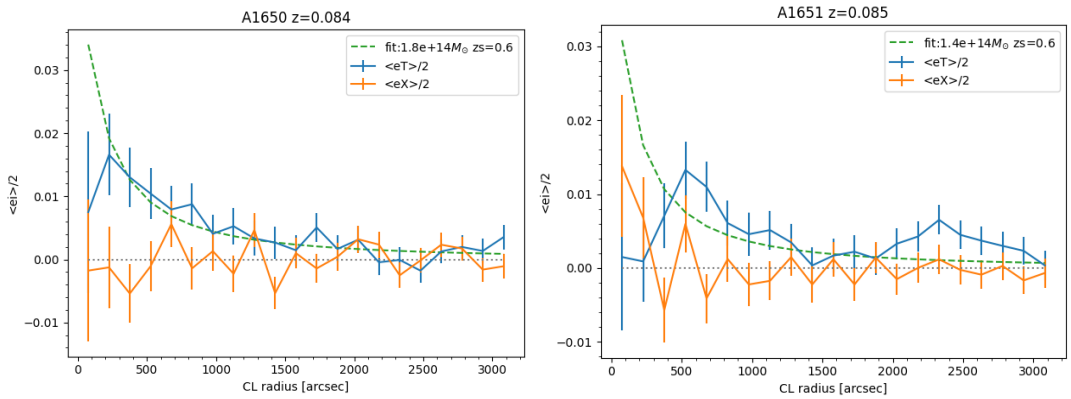

Figure 13: Comparison of shear profiles between A160(left) and A1651(right). Both profiles share the same trends of eT approaching zero as r gets large, and eX remaining around zero, however they differ as r approaches zero.

To be more precise, A1650 has a higher average tangential ellipticity close to r=0 when compared with A1651. This suggests that there is a higher degree of co-location between the X-ray center and gravitational lensing center in the non-merging galaxy cluster, A1650, which agrees with our original expectation. The degree of co-location, of course, can also be compared directly when looking at the topologies. In doing so, as seen in Figure 14, we can see that there is indeed a higher degree of co-location in the non-merging cluster. Despite the non-merging cluster's higher degree of co-location, however, there is still a noticeable difference in the X-ray and gravitational lensing centers, suggesting that there is still a degree of misalignment occurring.

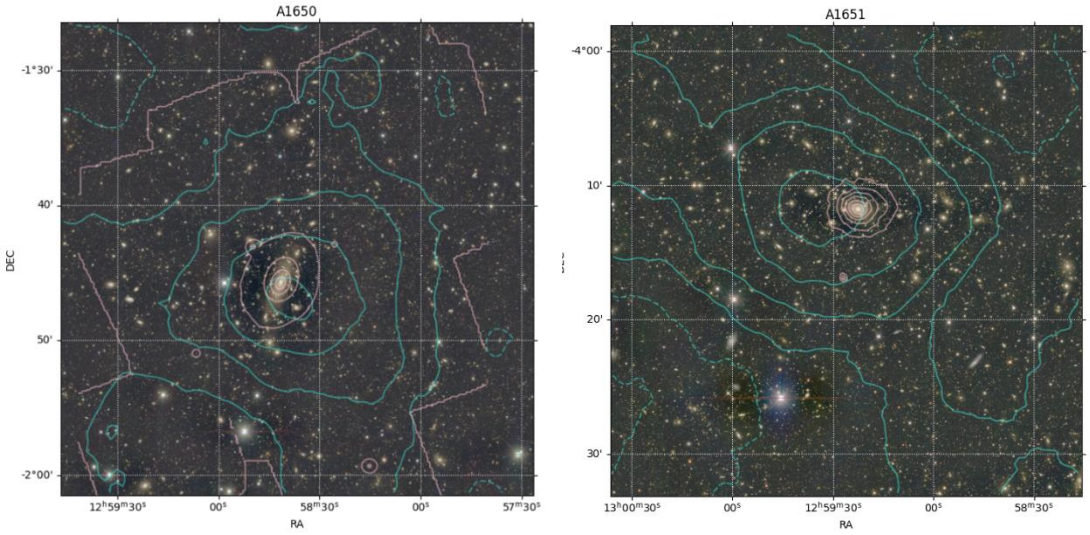

Figure 14: A1650(left) and A1651(right) topological maps compared. The degree of co-location between the X-ray center and gravitational lensing center is higher in the non-merging cluster, as we expected. Small X-ray dots in A1650's map represent active galaxies, which may or may not be associated with the cluster.

Furthermore, we can look farther out on the topological maps in order to discern any differences seen in terms of the macroscopic structure of the dark matter within the cluster. In doing so in Figure 15, we can see that there are more local sub-maxima within the merging cluster, suggesting that A1651 has a lumpier dark matter distribution. This difference in lumpiness agrees with our original expectations, as the merging galaxy cluster has not had enough time to develop a smooth distribution due timescale at which galaxy cluster merging occurs.

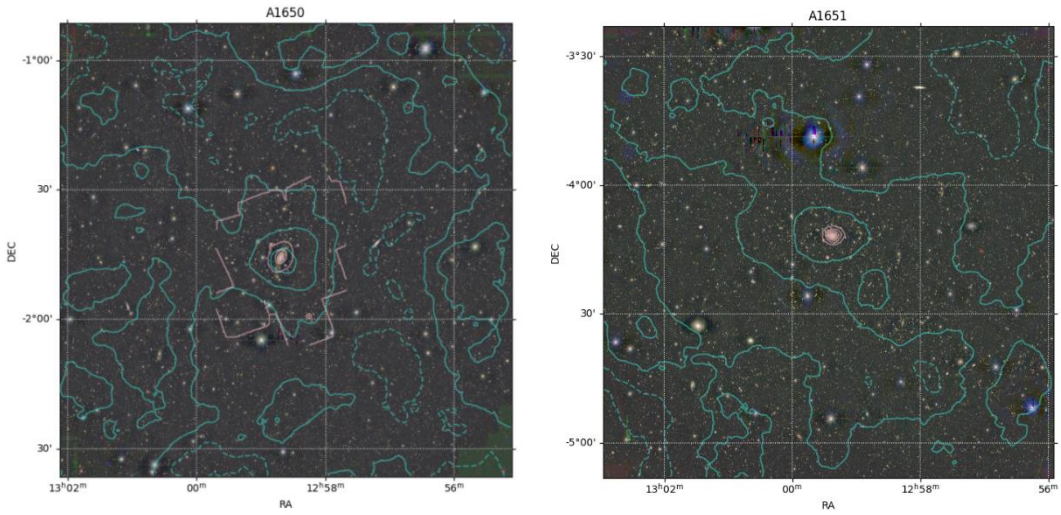

Figure 15: Zoomed out topology maps of both A1650(left) and A1651(right). In looking at the distribution of gravitational lensing signals, we can see that A1651 has a lumpier distribution. The additional pink lines in A1650's topology represents the edge of the cluster's X-ray measurements.

With respect to the parameterization of this lumpiness, we expect that if dark matter doesn't share any interaction with baryonic matter, then the timescale of the merger event with respect to the dark matter should be exclusively related to the tidal effects on the dark matter. It should be noted, however, that without further measurements made on the distance and color of the clusters, we cannot distinguish sub-clumps of dark matter which may not be a part of the cluster, but rather behind it still contributing to the gravitational lensing signal.

Chapter 6. Conclusions:

In comparing both the dark matter distribution and degree of co-location between A1651 and A1650, we found that the results agreed with our expectations in that merging clusters appear to show lower degrees of co-location and lumpier dark matter distributions. It should be noted, however, that comparing only two clusters can yield no definitive conclusions. In order to draw any substantial conclusions, the subject would be greatly benefitted by a dramatic increase in sample size, as well as further measurements on distance and color. In this sense, this paper acts as a prelude to the creation of an entire catalogue of clusters in which the same measurements are made. In doing so, we can later extend the study of the subject further to include variations in mass, mass distribution, and more specific characterizations of galaxy clusters to learn more about both how dark matter is distributed and how it interacts with our world.

References:

Wittman, David. “Weak Lensing.” ArXiv.org, 2 Aug. 2002, arxiv.org/abs/astro-ph/0208063.